Formulation of stress concentration factors for concrete-filled steel tubular (CFST) K-joints under three loading conditions without shear forces

Jian Zheng, Shozo Nakamura*, Toshihiro Okumatsu, Takafumi Nishikawa

Dept. of Civil and Environmental Eng., Nagasaki University, 1-14, Bunkyo-machi, Nagasaki 852-8521, Japan.

*Corresponding author：Shozo Nakamura

Tel: +81 95-819-2613

E-mail address: shozo@nagasaki-u.ac.jp

First author: Jian Zheng

E-mail address: zhengjianfzu@163.com

Third author: Toshihiro Okumatsu

Email address: okumatsu@nagasaki-u.ac.jp

Forth author: Takafumi Nishikawa

E-mail address: nishikawa@nagasaki-u.ac.jp

Abstract

Concrete-filled steel tubular (CFST) K-joints have been widely applied to CFST trussed arch bridges in China, which are comprised of a concrete-filled circular hollow section (CHS) chord and two CHS braces. It has been experimentally revealed that hot spot stress (HSS) of CFST K-joints is significantly lower than those of empty tubular K-joints in the reported researches. However, no parametric formulae on stress concentration factors (SCFs) of CFST K-joints have been established. In present study, three-dimensional FE models for determining the SCF distributions around the chord-brace intersections of CFST K-joints were developed first. The validity of the FE modelling has been examined by comparing with the published experimental results. Then 272 FE models of CFST K-joints with different geometric dimensions were prepared and provided for the parametric study to demonstrate the influence of four key geometric parameters, i.e. diameter ratio (β), diameter to thickness ratio of chord (2γ), thickness ratio (τ) and the angle (θ) between the axis of the chord and brace, on SCFs around the chord-brace intersection. The analysis was performed under three loading conditions, i.e. the basic balanced axial forces, axial compressive force in the chord and in-plane bending in the chord. Finally, parametric formulae to determine the SCFs in CFST K-joints were proposed by the multiple regression analysis, and their accuracy was demonstrated through the comparison of SCFs obtained by the proposed formulae and FEA.

Key words: CFST K-joints; Stress concentration factors; Hot spot stress; Fatigue; Finite element analysis; Parametric formulae.

1 Introduction

More than 100 concrete-filled steel tubular (CFST) trussed arch bridges (see Fig. 1) have been constructed and come into service, accounting for about 38% of all available CFST arch bridges in China [1]. The arch ribs in the trussed arch bridges comprise concrete-filled circular hollow section (CHS) chords with CHS braces. In general, full-penetration butt welds are used to connect them and to form a variety of CFST joints geometries. CFST K-joints whose three-dimensional diagram is shown in Fig. 2 are the most widely used for the connections of concrete-filled chords. CFST K-joints can enhance the performance of load transfer among arch ribs and improve the compressive strength and ductility of arch ribs. Whereas, much greater axial stiffness of the brace relative to the radial stiffness of the chord tube could lead to high stress concentration at the joint. In fact, fatigue damage of CFST K-joints has been observed in a practical bridge in Fujian Province, China [2]. Fig. 3 shows one of the fatigue cracks. The Chinese specification of CFST arch bridges [3] specifies only the allowable nominal stress amplitude for the fatigue life estimation of CFST joints since very few fatigue studies on them are available.

Hot spot stress (HSS) is widely used to evaluate fatigue life for tubular joints. The stress concentration factors (SCFs) are very simple and effective indices to predict the HSS. Numerous published studies [4–9] formulates the SCF for CHS joints based on the practical method of HSS. Their research outcomes have been widely adopted in many current design specifications [10–14]. However, there has been very limit effort to develop SCF formulae for CFST K-joints. Tong et al. [15] experimentally demonstrated that the SCFs of CFST K-joints are smaller and have more uniform distribution than those of CHS K-joints. Udomworarat et al. [16, 17] revealed that CFST K-joints have less SCFs values than CHS K-joints by using the experimental and finite element (FE) methods. Huang et al. [18] also experimentally found that CFST K-joints have more uniform strain distribution and lower peak strain than those in CHS K-joints with the same geometry by comparison of their principal strain distributions around the chord-brace intersections. Contribution of filled-concrete to reduce the SCFs for tubular joints was supported by the other researches such as in [19–25] through the comparison of SCFs between CFST joints and CHS joints with various types of tubular joints.

Concerning the studies on the parametric formulae of SCFs, Wang [26] and Chen [27] calculated the SCFs of CFST T-joints with the published formulae of CHS T-joints. In those studies, they considered the improvement of the local stiffness around the chord-brace intersection due to the filled-concrete by using the equivalent thickness. Musa et al. [28] proposed the parametric equation of the maximum SCF around the intersection of CFST T-joints under axial tension in the brace. In our previous researches [29], the special SCF parametric formulae were developed and proposed for CFST T-joints under several loading conditions. Furthermore, the SCF formulae of concrete-filled and PBL-stiffened rectangular hollow section cross-joints under axial tension in the brace were proposed [30]. Nevertheless, the SCF formulae for CFST K-joints have been not proposed. Moreover, the validity ranges of diameter to thickness ratio of chord (2γ) in [15] and thickness ratio (τ) in [21] do not match the practical ranges of geometric parameter in the joints of CFST arch bridges. Therefore, the development of a series of parametric formulae for calculating SCFs has been awaited to simplify HSS calculations for CFST K-joints.

In the present research, the FE models of CFST K-joints were developed in an attempt to replicate the published experimental results on SCF distributions [21] around the chord-brace intersections. After validating these FE modelling through the comparison with test results, they were employed for the parametric analysis. The loading conditions considered in the parametric analysis include the basic balanced axial forces, axial compressive force in the chord and in-plane bending in the chord. Parametric formulae to determine SCFs were derived as functions of four geometric parameters, i.e. the diameter ratio β (= d/D), diameter to thickness ratio of chord 2γ (= D/T), thickness ratio τ (= t/T) and the angle (θ) between the axis of the chord and brace (see Fig. 4). Finally, their accuracy was demonstrated through the comparison of SCFs obtained by the proposed formulae and FEA.

2 Validity of FE modelling

2.1 Outline of the target experiment

The experiments to investigate the SCF distribution along chord-brace intersection of CFST K-joints were carried out in Zhejiang University and published in [21]. The geometry and material properties of CFST K-joints specimens are listed in Table 1. The weld profile with full penetration was determined and specimen preparation was carried out in accordance with the American Welding Society (AWS) specification [11]. They were tested with one brace in axial tension, while another brace was fixed on the test rig by bolts in the end. Both ends of the chord were fixed by bolts for all test specimens. The loading method is shown in Fig. 5.

The specimens were loaded within elastic range to obtain the SCF distribution along the brace-chord intersections. Strain gauges were placed around the intersection to measure the strains perpendicular and parallel to the weld toe in the test specimens. The arrangement of strain gauges followed the linear extrapolation region recommended by CIDECT Design Guide [14]. The measured strains were used to determine hot spot strains, which were converted to the SCFs based on the provision in [10].

2.2 FE modelling

The numerical replication on SCF distribution around the chord-brace intersection of CFST K-joint specimens was carried out with FE analysis software MSC.Marc. The analysis assuming the linear elastic material and nonlinear contact properties was executed to replicate the experiments. Whole components, i.e. steel tube, filled-concrete and weld bead, were modelled by eight-node hexahedron solid element with the function of "assumed strain", which can avoid the one order element shear locking caused by full-integration. The axial tension were applied to the end in the vertical brace. The material properties in the verification models are given in

Table 1.

The dimensions of weld leg were set to t and $0.5t$ on the brace and chord sides, respectively, according to AWS specifications [11]. Around the chord-brace intersection, edge length of the elements was set to approximately 2 mm. The tubes were divided into elements in the thickness direction so as to make their edge length ratio approximately 1. These mesh specifications and generation process around the intersection are validated for the calculation of HSS around the intersection of CFST T-joints [29]. Around the intersection in the models with full penetration welds, elements of weld bead share the nodes on interfacing areas with the elements of both chord and braces.

"Touch" function was employed for the simulation of the contact behavior between steel pipe and in-filled concrete in the verification models, which allows them to touch and separate each other in normal direction, and to slide with friction behavior in tangential direction. In a structural analysis of MSC.Marc [31], "touch" function triggers the local application of a nonpenetration constraint still allowing relative sliding of the contact bodies in the contact interface. The nonpenetration constraint is applied through a tying or boundary condition on the displacement components normal to the contact surfaces. No bonding force between contact bodies was assumed in separation. The friction coefficient (μ) between concrete and steel is from 0.2 to 0.6 in general [32], and it does not significantly change the HSS around the intersection of CFST T-joints [29, 33]. Therefore, it was arbitrarily set to 0.3 as the previous study.

Fig. 6 shows the FE meshes of whole model and mesh details around the intersection. The ends of concrete-filled chord and horizontal brace are fixed. "RBE2" function in MSC.Marc was adopted to set the boundary conditions and loads, which defines a rigid kinematic link between a single retained node with dependent degrees of freedom specified at an arbitrary number of tied nodes [34]. The tied nodes are the nodes at the end of tube, and the retained node is the independent one at the center of the tube end section. The boundary conditions and loads were directly applied to the retained node.

2.3 Comparison of FE results with the experimental ones

The calculated methods of SCF in the FE replication are the same as those in the tests [21]. The comparison of SCF between the experimental and FEA results is shown in Table 2. The difference from -27% to +50% can be observed between FEA and test results. Except the SCFs at chord saddle in K-300-4 and at brace crown toe in K-300-4R, the differences are not more than 20%. When comparing the SCFs between specimens K-300-4 and K-300-4R having the same geometric parameters, the SCFs at chord show 33% difference. It indicates that such amount of difference in SCFs can occur even in the experiment due to some kinds of errors. Considering this fact, it can be thought that the FEA relatively well reproduce the test results.

To sum up in conclusion, combined with the finding that the FE modelling has sufficient accuracy to evaluate the SCFs of CFST T-joints under axial loading in the brace in the previous research [29], it can be thought that the FE modelling is also applicable to the evaluation of SCFs distribution of CFST K-joints.

3 Parametric analysis

3.1 Description of parametric analysis

3.1.1 FE models

The parametric equations of SCF for CHS K-joints [14] and the published research [15] indicate that the geometric parameters β, 2γ, τ and θ are the key to determination of SCFs for CFST K-joints. Ranges of the four key parameters for the parametric analysis were set to β = [0.3 – 0.6], 2γ = [40 – 80], τ = [0.4 – 1.0] and θ = [30° – 60°] referring to [33]. In addition, the following limitation are also adopted for the parametric analysis, i.e. (1) equal braces; (2) equal angles between the axis of the chord and braces ($\theta = \theta_1 = \theta_2$); (3) no eccentricity ($e = 0$ or $\rho = 0$); (4) the gaps are positive ($g > 0$), but $\geq 2t$; (5) full penetration butt welds are adopted for the chord-brace intersection.

The combination of geometric parameters is listed in Table 3. A total of 272 models, 240 models for developing SCF formulae and 32 models for additional validation of the formulae, were prepared. The parameters of standard model, which were determined in reference to typical dimensions of CFST trussed arch bridges in China, were set as listed in Table 4. They were determined in reference to the typical dimensions of the existing bridges in China [1]. Length of the brace (l) and length of the chord (L) were unchanged during the parametric analysis at $3d$ and $6D$, respectively. The dimensions of weld leg were set to t and $0.5t$ on the brace and chord sides, respectively, according to AWS specifications [11].

The existing researches [26, 28, 29] suggested that the effect of Young's modulus of common-used concrete on the SCFs of CFST joints can be neglected. The Young's modulus of concrete was set to the value corresponding to the strength of 50 MPa [35] since the concrete with the strength between 30 and 60 MPa has been generally used for the bridges in China [1]. The load in the concrete-filled chord was applied through the loading rigid plates set at the chord ends. The thickness of loading rigid plates are 20 mm, and their diameters are the same as the chord diameter (D). The material properties were set as shown in Table 5.

The setting used in the FE models for the type of analysis, the element types, the mesh specification and generation process, and the modeling of the chord tube-concrete interface are the same as those described in Section 2.2. "Glue" function, which does not allow contact bodies to have any relative displacements, i.e. binds contact bodies together, was adopted to simulate the interface behavior between loading rigid plate and concrete-filled chord. "Glue" function in MSC.Marc suppresses all relative motions between contact bodies through tyings or boundary conditions applying them to all displacement degrees of freedom of the nodes in contact [31]. The chord is simply supported and chord torsion is fixed. The tied nodes of "RBE2" function are the nodes at the end of brace or loading rigid plate, and the retained node is the independent one at the center of the brace end section or loading rigid plate. The boundary conditions were directly applied to the retained node.

3.1.2 Loading conditions

Three loading conditions, i.e. (1) basic balanced axial forces; (2) axial compression in the chord; (3) in-plane bending in the chord were taken into account for the parametric analysis referring to [14]. Under basic balanced axial forces, the maximum SCFs can occur at following locations; chord crown toe (CC), chord saddle (CS), chord crown heel (CH) around the tensile and compressive braces, and brace crown toe (BC), brace saddle (BS) and brace crown heel (BH) in tension and compression. Axial compression and in-plane bending in the chord always induce the maximum SCFs at location CC or CH, while the SCFs at other locations are very small. Therefore, the SCFs were calculated at these locations. The schematic diagram and possible positions of hot spot for each loading condition are shown in Table 6. The values of F_b, F_c and M_c in Table 6 are 2×10^5 N, 1×10^6 N and 1×10^8 N·mm, respectively. The applied method of loads is the same as those for the boundary conditions described in Section 3.1.1.

3.1.3 HSS calculation and definition of SCFs

CIDECT Design Guide [14] specifies the boundary of extrapolation region as shown in Fig. 7 and Table 7. The HSS around the chord-brace intersection was obtained by linear extrapolation using the stresses at two nodes whose positions are approximately $0.4T$ (but $\geq$ 4 mm) and $1.0T$ away from the weld toe, respectively. The SCF was defined as the ratio of the HSS at the joint to the nominal stress [14].

Referring to the nominal stress for CHS K-joints [36], the nominal stresses of

CFST K-joints under the basic balanced axial forces, axial compression in the chord (F_c) and In-plane bending moment in the chord (M_c) were determined as F_b / A_b, F_c / A and M_c / W, respectively. A_b is the area of the brace tube section. A and W are the area and section modulus of the equivalent steel tube section of the concrete-filled chord, respectively.

3.2 Results and discussions

3.2.1 Hot spot of each member under basic balanced axial forces

The contour plot of principal stress around the chord-brace under basic balanced axial forces is shown in Fig. 8. It shows the stress along the intersection in chord-side is generally larger than that in brace-side. By comparing the stress among the hot spot in each member, it can be observed that the maximum SCF generally occurs at the chord around the tensile brace, which is much larger than that around the compressive brace. Due to low adhesion between the chord tube and concrete, the inner wall of chord would tend to separate from the concrete filling around the chord-brace intersection under tensile brace, while the concrete filling would provide strong support for the chord wall under the compressive brace, as illustrated in Fig. 9. Consequently, local bending deformation around the intersection under tension is much larger than that under compression, resulting in higher SCF under tension than that under compression.

The position of hot spot in each member along the chord-brace intersection under basic balanced axial forces is summarized in Table 8. In general, the hot spot in the chord is mainly at either location CC or CS around the tensile brace, and always at location CC around the compressive brace. The hot spot locations in the tensile brace vary depending on the joint parameters. The location BC or BS is, however, often the hot spot. In the compressive brace, the hot spot is mainly at either location BC or BH. The hot spot positions between the intersections under tension and compression can be different by the influence of concrete filling and the behavior of the chord tube-concrete interface explained above. Hence, the SCF formulae need to be developed independently for each possible hot spot position.

3.2.2 Comparison of SCF between locations CC and CH under chord loading

The contour plot of principal stress around the chord-brace under chord loading is shown in Fig. 10. It shows the stress concentration generally occurs at locations CC and CH. The position of hot spot in each member along the chord-brace intersection under chord loading is summarized in Table 9. In general, the hot spot in the chord is at either location CC or CH, but mainly at location CH.

The hot spot can occur at location CC or CH under the chord loading. The comparisons of SCFs between locations CC and CH under the chord loading are shown in Fig. 11. It can be observed that the SCFs at locations CC and CH are not very different. The mean of their ratio is close to 1 and their maximum difference is approximately 20%. Considering relatively small SCF-values, it can be thought that independent formulation of SCFs for both locations is not necessary.

4 Proposed formulae and their accuracy verification

4.1 Formulation

A SCF formula for CFST K-joints was assumed in the form of Eq. (1) based on the proposed parametric formulae for CHS K-joints in CIDECT Design Guide [14, 37].

$$\mathrm{SCF} = \mu \left(\frac{\gamma}{\gamma_0} \right)^a \left(\frac{\tau}{\tau_0} \right)^b \mathrm{SCF}_0 \tag{1}$$

Where, γ_0 and τ_0 are determined from the standard CFST K-joint in Table 4, i.e. $\gamma_0 = 20$ and $\tau_0 = 0.4$; SCF_0 is the SCF obtained from the basic combination of geometric parameters, which is derived as a function consisting of parameter β and obtained by the method of a second order polynomial; The constants μ, the exponents a and b would be determined by the multiple regression analysis.

Since the analysis results are obtained for the sets of θ = 30°, 45° and 60°, the multiple regression analysis using the FE results of 240 models with θ = 30°, 45° and 60° in Table 3 has been carried out for each loading condition, location and θ-value. Their results are shown in Table 10.

For the other θ-value, the SCF formula is assumed as shown in Eq. (2).

$$\mathrm{SCF}_\theta = A\theta^2 + B\theta + C \tag{2}$$

The coefficients A, B and C in Eq. (2) can be obtained for each combination of β-, γ-, τ-values using the $\mathrm{SCF}_{\mathrm{FEA}}$ values for θ = 30°, 45° and 60° as SCF_θ.

By assuming the coefficients A, B and C in Eq. (2) as the ternary linear equations in terms of SCF_{30}, SCF_{45} and SCF_{60}, where SCF_{30}, SCF_{45} and SCF_{60} are the SCF value under θ = 30°, 45° and 60°, respectively, Eq. (3) has been obtained.

$$
\begin{aligned}
A &= \frac{\mathrm{SCF}_{60} - 2\mathrm{SCF}_{45} + \mathrm{SCF}_{30}}{450} \\
B &= \frac{-5\mathrm{SCF}_{60} + 12\mathrm{SCF}_{45} - 7\mathrm{SCF}_{30}}{30} \\
C &= 3\mathrm{SCF}_{60} - 8\mathrm{SCF}_{45} + 6\mathrm{SCF}_{30}
\end{aligned}
\tag{3}
$$

The proposed SCF formulae are valid for the ranges shown below since they are proved only for these ranges.

$$0.3 \le \beta \le 0.6,\ 40 \le 2\gamma \le 80,\ 0.4 \le \tau \le 1.0,\ 30° \le \theta \le 60°$$

4.2 Validation of the accuracy

A comparison of SCFs obtained by the proposed formulae in Eq. (1) and Table 10, $\mathrm{SCF}_{\mathrm{FOR}}$, and the FE analysis, $\mathrm{SCF}_{\mathrm{FEA}}$, is shown in Fig. 12 to evaluate the accuracy of the formulae for the cases with θ-values of 30°, 45° and 60°. The acceptance of the proposed formulae is assessed according to the statistical measures, i.e. the ratio $\mathrm{SCF}_{\mathrm{FOR}}/\mathrm{SCF}_{\mathrm{FEA}}$ and the coefficients of variance (COV). Overall, there are good agreements between the two sets of SCFs. The mean values and COVs of $\mathrm{SCF}_{\mathrm{FOR}}/\mathrm{SCF}_{\mathrm{FEA}}$ listed in Fig. 12 indicate the accuracy of the formulae for all locations and loading conditions considered in this study.

The parametric formulae for SCF_{θ} shown in Eqs. (2) and (3) were verified using FEA results of 32 models with other θ-values in Table 3, for all locations. The comparisons for all loading conditions are shown in Fig. 13, which shows that $\mathrm{SCF}_{\mathrm{FOR}}$ is in good consistent with $\mathrm{SCF}_{\mathrm{FEA}}$.

In order to determine the SCFs caused by the combination of three loading conditions in Table 6, ten models with different geometric parameters are employed to predict HSS, $\sigma_{h,FEA}$, and make a comparison with HSS determined by proposed formulae, $\sigma_{h,FOR}$. The geometric parameters of ten models are listed in Table 11. The load values of three loading conditions are the same as those in the parametric analysis. Total HSS of a CFST K-joint at a specific hot spot location can be determined by the following equation [14]:

$$\sigma_{h,FOR} = SCF_{a0} \times \sigma_{n,a0} + SCF_{a1} \times \sigma_{n,a1} + SCF_{m1} \times \sigma_{n,m1} \quad (4)$$

Where, $\sigma_{n,a0}$ is the nominal stress under basic balanced axial forces, $\sigma_{n,a1}$ is the nominal stress under axial compression in the chord, $\sigma_{n,m1}$ is the nominal stress under in-plane bending in the chord, SCF_{a0}, SCF_{a1} and SCF_{m1} are the corresponding SCFs.

A comparison between $\sigma_{h,FEA}$ and $\sigma_{h,FOR}$ for the all hot spot locations of the models in Table 11 under loading combination is shown in Fig. 14. Positive values represent the tensile stress, and negative values represent the compressive stress. Fig. 14 shows good agreement between $\sigma_{h,FOR}$ and $\sigma_{h,FEA}$, which indicates that the superposition theory can be applied to predict the HSS for CFST K-joints under the combination of three loading conditions.

Consequently, the proposed formulae are thought to be applicable for the determination of SCFs in CFST K-joints under three loading conditions with sufficient accuracy.

5 Concluding remarks

In this study, the developed finite element (FE) models for concrete-filled steel tubular (CFST) K-joints was verified first. Then, an extensive parametric analysis using the validated FE modelling was performed to evaluate the influences of the key geometric parameters β, 2γ, τ and θ on the stress concentration factors (SCFs). Finally, based on the results of 816 analyses, a series of parametric formulae to determine the SCFs of CFST K-joints under three loading conditions were proposed. The following conclusions can be drawn from this research:

(1) Under basic balance axial forces, the SCFs around the intersection in tension are much larger than those in compression. In the chord around the intersection with the tensile brace, the hot spot is mainly located at either the crown toe or saddle. In the chord around the intersection with the compressive brace, the hot spot always locates at the crown toe. In the tensile brace, the hot spot locations vary depending on the joint parameters, although the crown toe or saddle is often the hot spot. In the compressive brace, the hot spot is mainly located at either the crown toe or crown heel.

(2) Under the axial compression or in-plane bending in the chord, the hot spot in the chord locates at either crown toe or crown heel, but mainly at crown heel, and their SCFs are very close.

(3) Parametric SCF formulae including the four key geometric parameters were proposed for CFST K-joints under three loading conditions with sufficient accuracy and reliability.

(4) The proposed parametric formulae in current research are valid under the

five limitations described in Section 3.1.1 and the validity ranges given in Section 4.1.

In the development of the SCF formulae, the concrete filling is assumed complete. However, it can be incomplete due to some causes such as creep, shrinkage, and entrapped air. It should be noted that the SCFs could be larger than that obtained by the formulae under such conditions [29].

Acknowledgments

This research was financially supported by China Scholarship Council (No. 201506650004). The authors would like to express the sincere gratitude to the supports.

References

[1] Wang Q, Nakamura S, Chen KM, Chen BC and Wu QX. Comparison between steel and concrete-filled steel tubular arch bridges in China. Proceedings of constructional steel, Japanese Society of Steel Construction, 2016; 24: 66–73.

[2] Wang Q, Nakamura S, Chen KM, Chen BC and Wu QX. Fatigue evaluation of K-joint in a half-through concrete-filled steel tubular trussed arch bridge in china by hot spot stress method. Proceedings of constructional steel, Japanese Society of Steel Construction, 2016; 24: 633–640.

[3] JTG/T D65-06-2015. Specifications for design of highway concrete-filled steel tubular arch bridge. China Communication Press, Beijing, China; 2015 [in Chinese].

[4] Kuang JG, Potvin AB, Leick RD. Stress concentration in tubular joints. In: Proceedings of the seventh annual offshore technology conference, OTC 2205. Houston, Texas; 1975. p. 593–612.
[5] Efthymiou M, Durkin S. Stress concentrations in T/Y and gap/overlap K-joints. Behavior of offshore structures: proceedings of the 4th international conference on behavior of offshore structures, Elsevier, Amsterdam, 1985 429–440.
[6] Hellier AK, Connolly MP, Dover WD. Stress concentration factors for tubular Y-and T-joints. International Journal of Fatigue 1990; 12(1): 13–23.
[7] Smedley PA, Fisher PJ. Stress concentration factors for simple tubular joints. In: Proceedings of the first international offshore and polar engineering conference. International society of offshore and polar engineers, Edinburgh, UK, 1991. p. 475–483.
[8] Mashiri FR, Zhao XL, Grundy P. Stress concentration factors and fatigue behaviour of welded thin-walled CHS–SHS T-joints under in-plane bending. Engineering Structures 2004; 26(13): 1861–1875.
[9] Zhao XL, Wilkinson T, Hancock GJ. Cold-formed tubular members and connections: Structural behaviour and design, Elsevier, Oxford, UK, 2005.
[10] API. American Petroleum Institute. Recommended practice for planning, designing and constructing fixed offshore platforms. 21st Ed., API Publishing Services, Washington DC; 2014.
[11] AWS. American Welding Society. Structural welding code-steel. AWS D1.1/1.1M. American Welding Society Inc, Miami; 2004.

[12] ABS. American Bureau of Shipping. Guide for buckling and ultimate strength assessment for offshore structures. American Bureau of Shipping, Houston; 2004.

[13] DNV. DNV recommended practice RP-C203. Fatigue strength analysis of offshore of steel structures. Det Norske Veritas, Norway; 2010.

[14] Zhao XL, Herion S, Packer JA, Puthli R, Sedlacek G, Wardenier J, et al., Design guide for circular and rectangular hollow section joints under fatigue loading, CIDECT, TUV, 2000.

[15] Tong LW, Sun CQ, Chen YY, Zhao XL, Shen B, Liu CB. Experimental comparison in hot spot stress between CFCHS and CHS K-joints with gap. In: Proceedings of 12th International Symposium on Tubular Structures; 2008. p. 389–395.

[16] Udomworarat P, Miki C, Ichikawa A, Sasaki E, Sakamoto T, Mitsuki K, Hosaka T. Fatigue and ultimate strengths of concrete filled tubular K-joints on truss girder. JSCE Journal of Structural Engineering 2000; 46(3): 1627–1635.

[17] Udomworarat P, Miki C, Ichikawa A, Sasaki E, Komechi M, Mitsuki K, Hosaka T. Fatigue performance of composite tubular K-joints for truss type bridge. JSCE Structural Engineering/Earthquake Engineering 2002; 19(2): 65s–79s.

[18] Huang WJ, Fenu L, Chen BC, Briseghella B. Experimental study on K-joints of concrete-filled steel tubular truss structures. Journal of Constructional Steel Research 2015; 107: 182–193.

[19] Wang K, Tong LW, Zhu J, Zhao XL, Mashiri FR. Fatigue behavior of welded

T-joints with a CHS brace and CFCHS chord under axial loading in the brace. Journal of Bridge Engineering 2011; 18(2): 142–152.

[20] Chen J, Chen J, Jin WL. Experiment investigation of stress concentration factor of concrete-filled tubular T joints. Journal of Constructional Steel Research 2010; 66(12): 1510–1515.

[21] Xu F, Chen J, Jin WL. Experimental investigation of SCF distribution for thin-walled concrete-filled CHS joints under axial tension loading. Thin-Walled Structures 2015; 93: 149–157.

[22] Kim IG, Chung CH, Shim CS, Kim YJ. Stress concentration factors of N-joints of concrete-filled tubes subjected to axial loads. International Journal of Steel Structures 2014; 14(1): 1–11.

[23] Diao Y. Experimental research on fatigue performance of tubular joints in concrete-filled steel bridges. Ph.D. thesis, Southwest Jiaotong Univ., Chengdu, China; 2012 [in Chinese].

[24] Mashiri FR, Zhao XL. Square hollow section (SHS) T-joints with concrete-filled chords subjected to in-plane fatigue loading in the brace. Thin-Walled Structures 2010; 48(2): 150–158.

[25] Liu YJ, Xiong ZH, Feng YC, Jiang L. Concrete-filled rectangular hollow section X joint with Perfobond Leister rib structural performance study: Ultimate and fatigue experimental Investigation. Steel and Composite Structures 2017; 24(4): 455–465.

[26] Wang K. Study on the hot spot stress and fatigue strength of welded circular

hollow section (CHS) T-joints with concrete-filled chords. Ph.D. thesis, Tongji Univ., Shanghai, China; 2008 [in Chinese].

[27] Chen J. Experimental and theoretical study of dynamic performance of concrete-filled steel tubular T-joints. Ph.D. thesis, Zhejiang Univ., Hangzhou, China; 2011 [in Chinese].

[28] Musa IA, Mashiri FR, Zhu XQ. Parametric study and equation of the maximum SCF for concrete filled steel tubular T-joints under axial tension. Thin-Walled Structures 2018; 129: 145–156.

[29] Zheng J, Nakamura S, Ge YJ, Chen KM, Wu QX. Formulation of stress concentration factors for concrete-filled steel tubular (CFST) T-joints under axial force in the brace. Engineering Structures 2018; 170: 103–117.

[30] Liu YJ, Jiang L, Xiong ZH, Zhang GJ, Fam A. Hot spot SCF computation method of concrete-filled and PBL-stiffened rectangular hollow section joint subjected to axial tensions. Journal of Traffic and Transportation Engineering 2017; 17(5): 1–15 [in Chinese].

[31] Marc® 2013.1, help system. Volume A: Theory and user information. MSC Software Corporation, 2013.

[32] Baltay P, Gjelsvik A. Coefficient of friction for steel on concrete at high normal stress. Journal of Materials in Civil Engineering 1990; 2(1): 46–49.

[33] Zheng J, Nakamura S, Chen KM, Wu QX. Numerical Parameter Analysis on Stress Concentration Factors of Concrete-filled Steel Tubular (CFST) K-joint under Axial Loading. In: Proceedings of the 2017 World Congress on Advances

in Structural Engineering and Mechanics. Seoul, Korea, 2017.

[34] Marc® 2013.1, help system. Volume C: Program input. MSC Software Corporation, 2013.

[35] JTG D62-2004. Code for design of highway reinforced concrete and prestressed concrete bridges and culverts. China Communication Press, Beijing, China, 2004 [in Chinese].

[36] Schumacher A, Nussbaumer A. Experimental study on the fatigue behaviour of welded tubular K-joints for bridges. Engineering Structures 2006; 28(5): 745–755.

[37] Shao YB. Proposed equations of stress concentration factor (SCF) for gap tubular K-joints subjected to bending load. International Journal of Space Structures 2004; 19(3): 137–147.

Table 1 Geometry and material properties of CFST K-joints specimens

Geometry										
Specimens	Chord			Brace			Geometric parameters			
	Steel grade	*D* (mm)	*T* (mm)	Steel grade	*d* (mm)	*t* (mm)	θ (deg.)	β	2γ	τ
K-300-4	Q235	300.24	4.18	Q345	132.71	6.08	45	0.443	75	1.5
K-300-4R	Q235	300.11	4.18	Q345	133.25	6.08	45	0.443	75	1.5
K-300-5	Q235	300.32	5.02	Q345	132.98	6.06	45	0.443	60	1.2
Material properties										
Material		Young's modulus (MPa)				Poisson's ratio				
Steel	Q235	197000				0.3				
	Q345	199000				0.3				
Concrete		37420				0.2				

Table 2 Numerical SCFs and comparison with experimental ones

Specimen		SCFs		
		Chord saddle	Brace crown toe	Brace saddle
K-300-4	Test	2.4	2.0	0.9
	FEA	3.6	1.6	0.9
K-300-4R	Test	3.2	2.2	1.1
	FEA	3.6	1.6	0.9
K-300-5	Test	3.9	2.1	1.3
	FEA	3.8	1.7	1.1

Table 3 Combination of geometric parameters

Number of Models	θ/°	β	2γ	τ
240	30, 45, 60	0.3, 0.4, 0.5, 0.6	40, 50, 60, 70, 80	0.4, 0.6, 0.8, 1.0
32	35, 40, 50, 55	0.3, 0.4, 0.5, 0.6	40, 80	1.0

Table 4 Geometric parameters of standard FE model

Structural dimensions						
D/mm	*d*/mm	*T*/mm	*t*/mm	*L*/mm	*l*/mm	*θ*/°
600	300	15	6	3600	900	45
Non-dimensional geometric parameters						
β	2γ	τ	ρ			
0.5	40	0.4	0			

Table 5 Material Properties for parametric analysis

Material	Young's modulus (MPa)	Poisson's ratio
Steel tube and weld bead	2.05×10^5	0.3
Concrete	3.45×10^4	0.2
Loading rigid plate	1.00×10^8	0.3

Table 6 Loading conditions and their hot spot locations

Loading condition	Hot spot locations
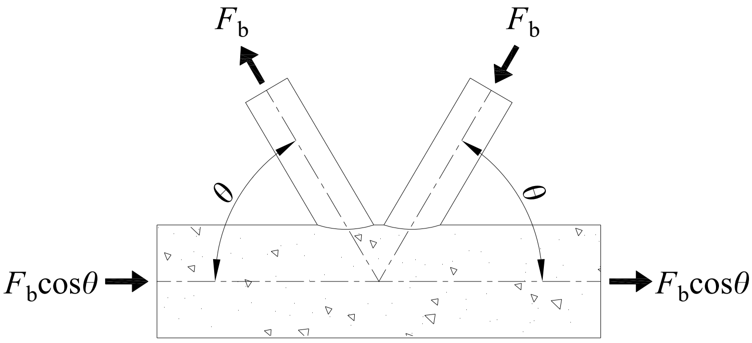 Basic balanced axial forces	CC, CS, CH BC, BS, BH
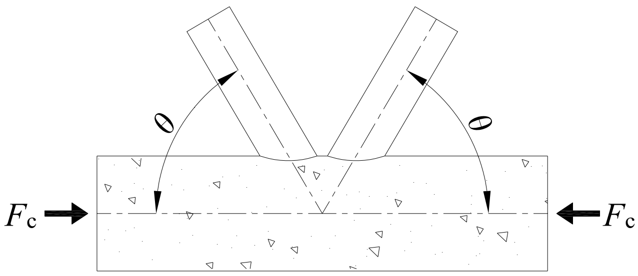 Axial compression in the chord	CC, CH
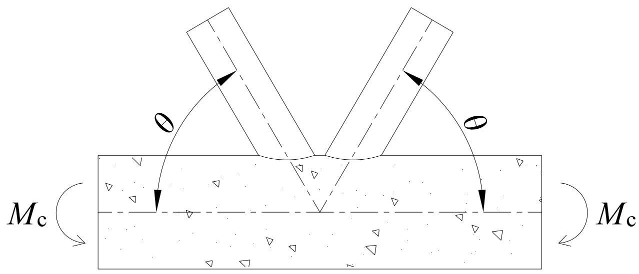 In-plane bending in the chord	CC, CH

Table 7 Boundaries of extrapolation region

Distance from weld toe	Chord		Brace
	Saddle	Crown	Saddle / Crown
Lr,min [*)]	$0.4T$		$0.4t$
Lr,max [**)]	$0.045D$	$0.4\sqrt[4]{0.25DTdt}$	$0.65\sqrt{0.5dt}$

[*)] Minimum value for Lr,min is 4mm, [**)] Minimum value for Lr,max is Lr,min + $0.6t$.

Table 8 Distribution of hot spot position in each member under basic balanced axial forces

Chord (tension)			
Location	CC	CS	CH
Percentage	55%	45%	0%
Chord (compression)			
Location	CC	CS	CH
Percentage	100%	0%	0%
Brace (tension)			
Location	BC	BS	BH
Percentage	35%	41%	24%
Brace (compression)			
Location	BC	BS	BH
Percentage	59%	0%	41%

Table 9 Distribution of hot spot position under the chord loading

Under axial compression in the chord		
Location	CC	CH
Percentage	32%	68%
Under in-plane bending in the chord		
Location	CC	CH
Percentage	36%	64%

Table 10 Proposed SCF formulae of CFST K-joints

Loading condition	Location		θ (°)	μ	a	b	SCF_0
Under basic balanced axial forces	Chord (ten.)	CC	30	0.565	0.693	0.637	$-1.453\beta^2+2.011\beta+1.539$
			45	0.815	0.425	0.806	$5.185\beta^2-3.154\beta+2.438$
			60	1.025	0.337	0.928	$-3.322\beta^2+3.711\beta+1.169$
		CS	30	0.395	0.508	0.997	$0.617\beta^2-1.634\beta+2.730$
			45	0.687	0.561	1.016	$0.939\beta^2-2.299\beta+2.965$
			60	1.024	0.498	1.031	$-0.962\beta^2-0.857\beta+2.729$
		CH	30	0.157	1.042	-0.434	$7.204\beta^2-10.020\beta+5.185$
			45	0.316	0.755	0.513	$5.151\beta^2-4.977\beta+3.259$
			60	0.488	0.691	0.958	$-1.822\beta^2+2.704\beta+1.306$
	Chord (comp.)	CC	30	0.263	0.359	0.439	$0.964\beta^2+0.653\beta+1.645$
			45	0.471	-0.115	0.743	$12.924\beta^2-6.421\beta+2.365$
			60	0.720	-0.214	0.902	$-3.554\beta^2+0.881\beta+2.519$
		CS	30	0.126	-0.309	0.866	$2.944\beta^2-3.567\beta+3.097$
			45	0.216	-0.086	0.867	$-3.597\beta^2+3.281\beta+1.419$
			60	0.329	-0.113	0.908	$-0.147\beta^2-1.658\beta+2.916$
		CH		SCFs can be de neglected since their values are very small.			
	Brace (ten.)	BC	30	0.651	0.072	-0.153	$8.506\beta^2-8.748\beta+4.239$
			45	1.061	-0.080	-0.198	$20.160\beta^2-18.630\beta+6.190$
			60	1.233	-0.125	-0.187	$6.487\beta^2-7.780\beta+4.250$
		BS	30	0.200	-0.236	1.144	$15.960\beta^2-19.725\beta+7.708$

			45	0.537	0.225	0.618	$12.380\beta^2-13.768\beta+5.694$
			60	0.908	0.307	0.487	$8.084\beta^2-9.048\beta+4.474$
		BH	30	0.629	-0.426	0.554	$4.446\beta^2-5.503\beta+3.655$
			45	0.795	-0.196	-0.352	$4.973\beta^2-5.919\beta+3.729$
			60	0.797	0.093	-0.201	$3.731\beta^2-4.086\beta+3.163$
	Brace (comp.)	BC	30	0.473	0.205	-0.182	$0.207\beta^2+2.233\beta+1.101$
			45	0.663	0.094	0.096	$7.712\beta^2-4.656\beta+2.586$
			60	0.841	-0.031	0.122	$-1.410\beta^2+0.857\beta+2.039$
		BS	30	0.101	-1.261	1.112	$11.957\beta^2-21.465\beta+9.745$
			45	0.303	-0.395	0.285	$0.640\beta^2-4.815\beta+4.243$
			60	0.500	-0.172	0.159	$1.567\beta^2-3.451\beta+3.358$
		BH	30	0.605	-0.267	0.480	$0.698\beta^2-1.113\beta+2.473$
			45	0.615	-0.269	0.311	$8.628\beta^2-8.756\beta+4.216$
			60	0.678	-0.173	0.231	$-1.118\beta^2+1.083\beta+1.874$
Under axial compression in the chord	Chord		30	0.628	-0.266	0.368	$4.369\beta^2-5.161\beta+3.513$
			45	0.571	-0.248	0.282	$1.717\beta^2-2.504\beta+2.885$
			60	0.554	-0.234	0.213	$0.507\beta^2-1.179\beta+2.546$
Under in-plane bending in the chord	Chord		30	0.671	-0.286	0.458	$2.605\beta^2-3.367\beta+3.083$
			45	0.605	-0.262	0.357	$2.140\beta^2-2.607\beta+2.837$
			60	0.583	-0.249	0.278	$0.294\beta^2-0.697\beta+2.373$

Table 11 Geometric parameters of the models

Model	θ (deg.)	β	2γ	τ
1	30	0.4	60	1.0
2	30	0.5	60	1.0
3	35	0.3	40	1.0
4	40	0.3	40	1.0
5	45	0.4	60	1.0
6	45	0.5	60	1.0
7	50	0.3	40	1.0
8	55	0.3	40	1.0
9	60	0.4	60	1.0
10	60	0.5	60	1.0

Fig. 1 CFST trussed arch bridge

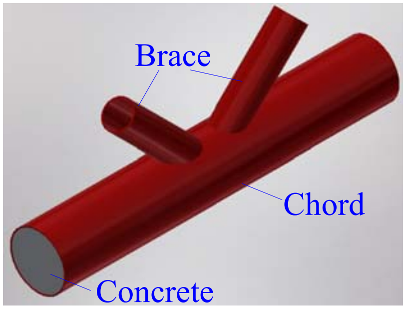

Fig. 2 Three-dimensional diagram of CFST K-joints

Fig. 3 Fatigue crack

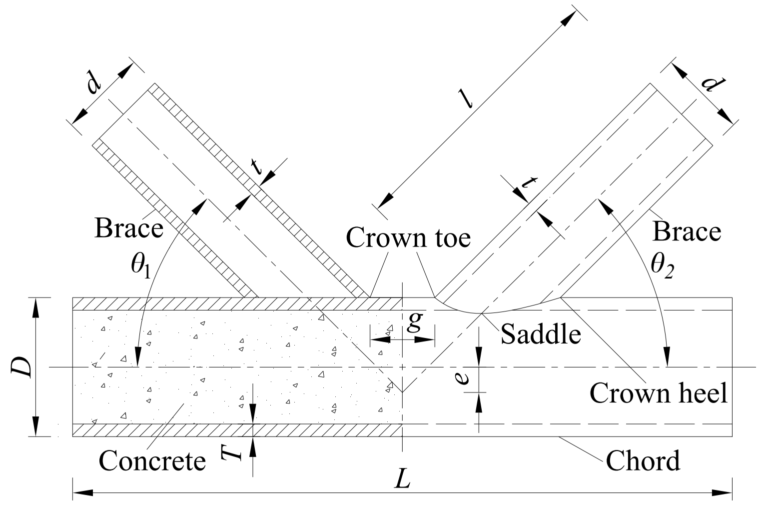

Fig. 4 Geometric parameters of CFST K-joints

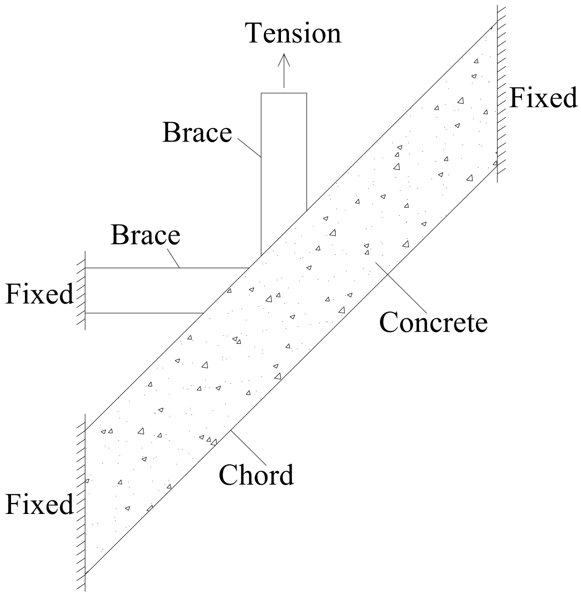

Fig. 5 Test loading method

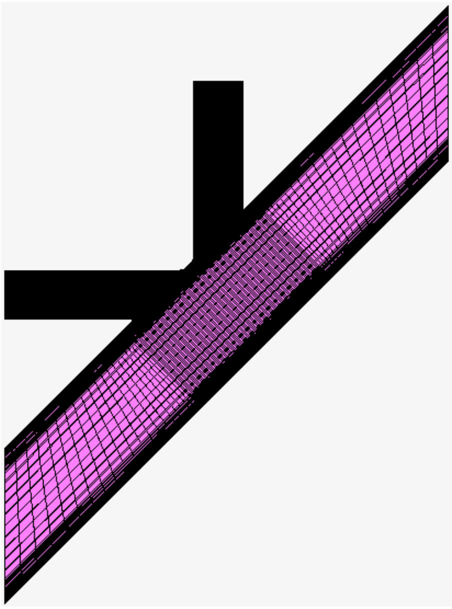

(a) FE model

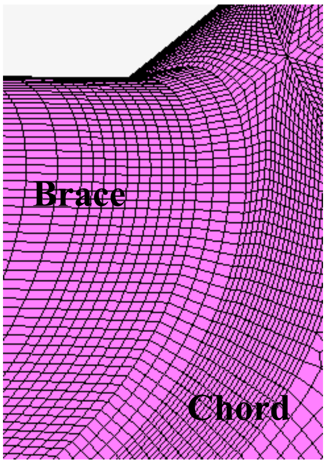

(b) Local mesh of steel tube around crown toe

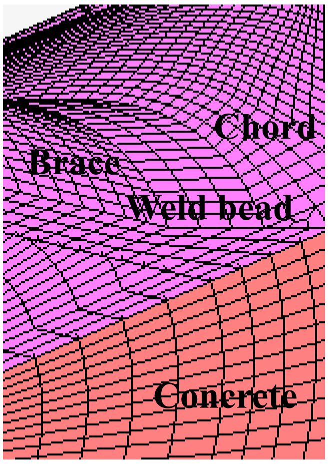

(b) Local mesh around crown toe

Fig. 6 FE model and local mesh of CFST K-joint

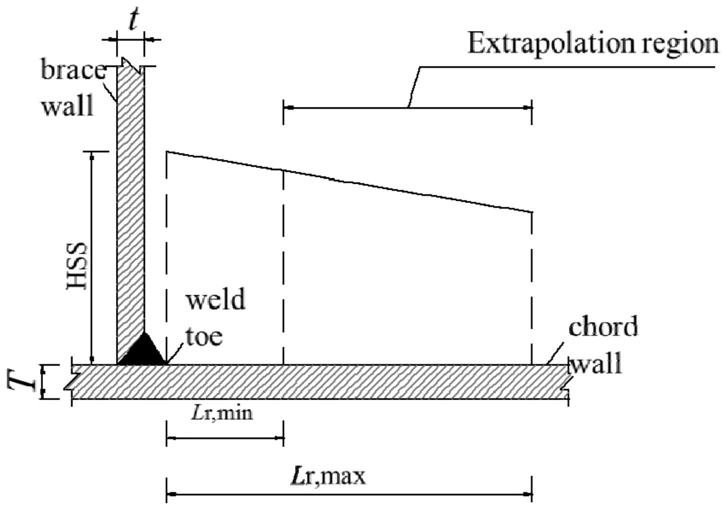

Fig. 7 Definition of extrapolation region

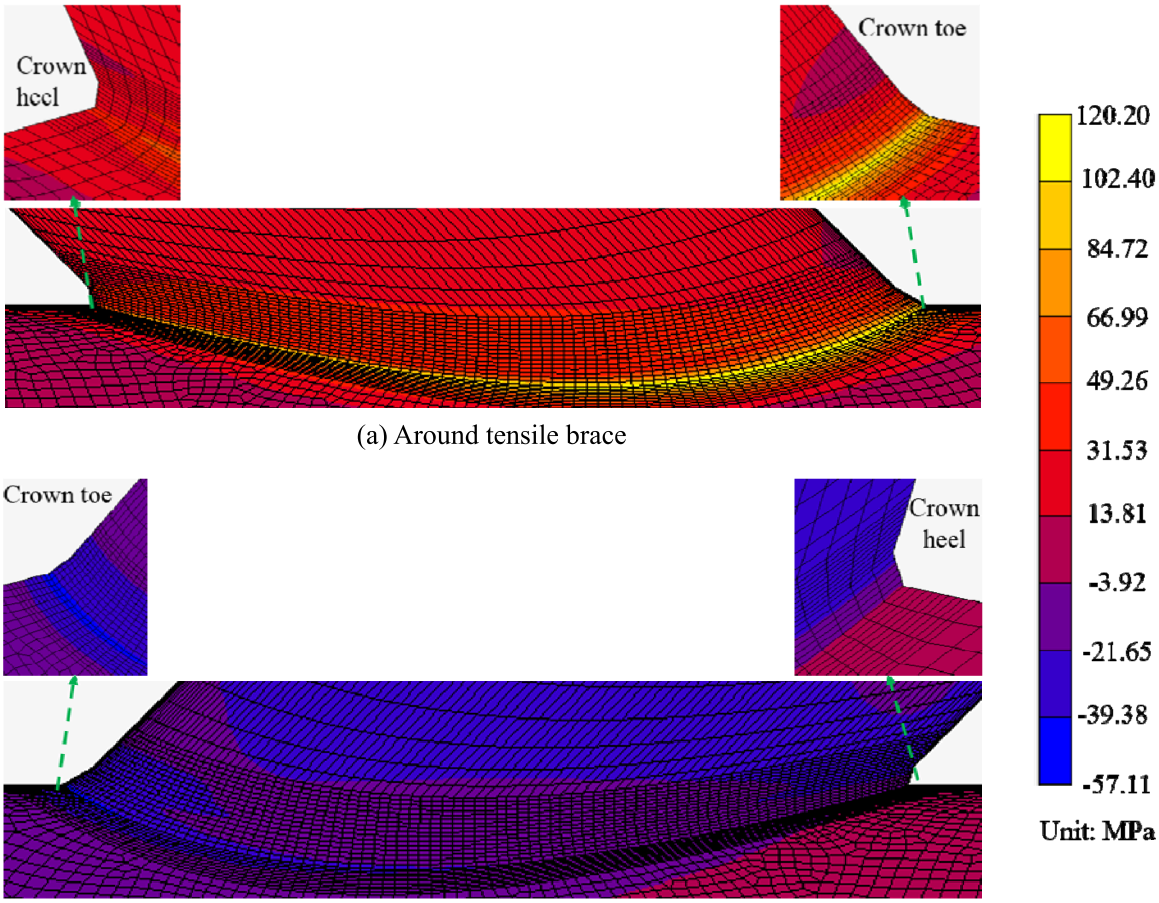

(b) Around Compressive brace

Fig. 8 Contour plot of the principal stress around the intersection under basic balanced axial forces

($\theta = 45°$, $\beta = 0.5$, $2\gamma = 60$, $\tau = 1.0$)

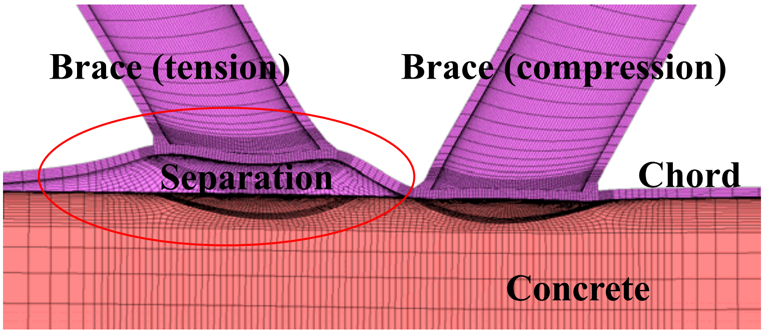

Fig. 9 Amplified deformation between chord tube and concrete

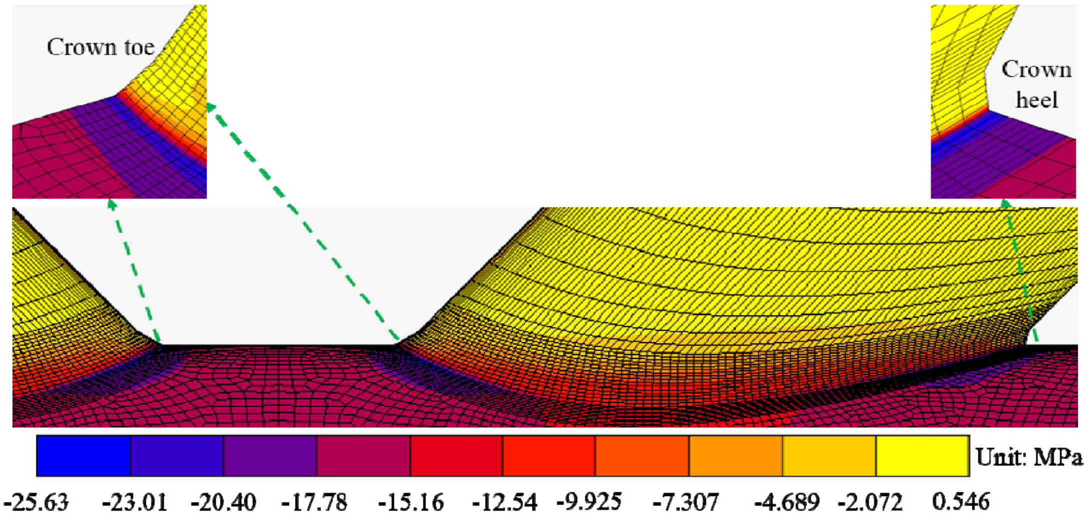

(a) Under axial compression in the chord

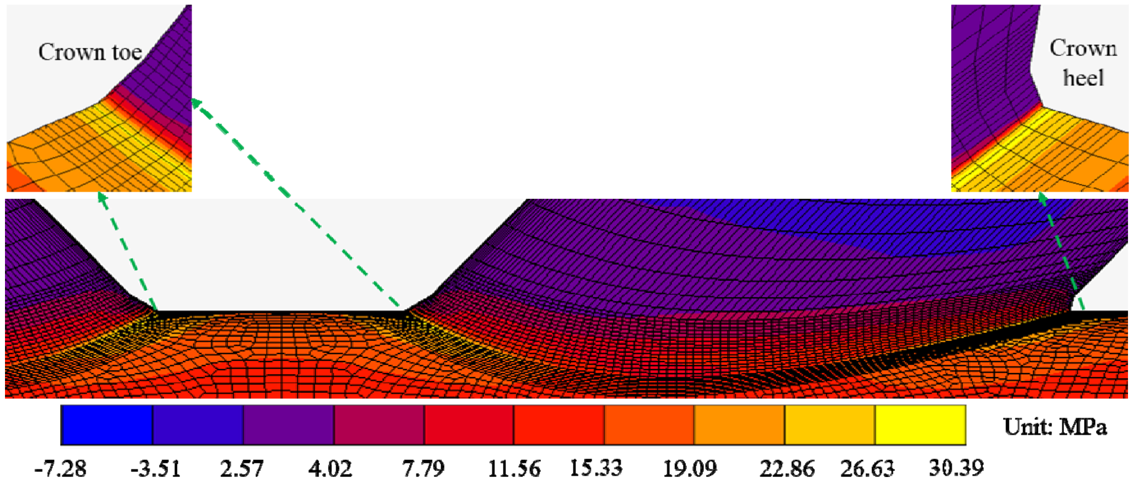

(b) Under in-plane bending in the chord

Fig. 10 Contour plot of the principal stress around the intersection under chord loading

($\theta = 45^\circ$, $\beta = 0.5$, $2\gamma = 60$, $\tau = 1.0$)

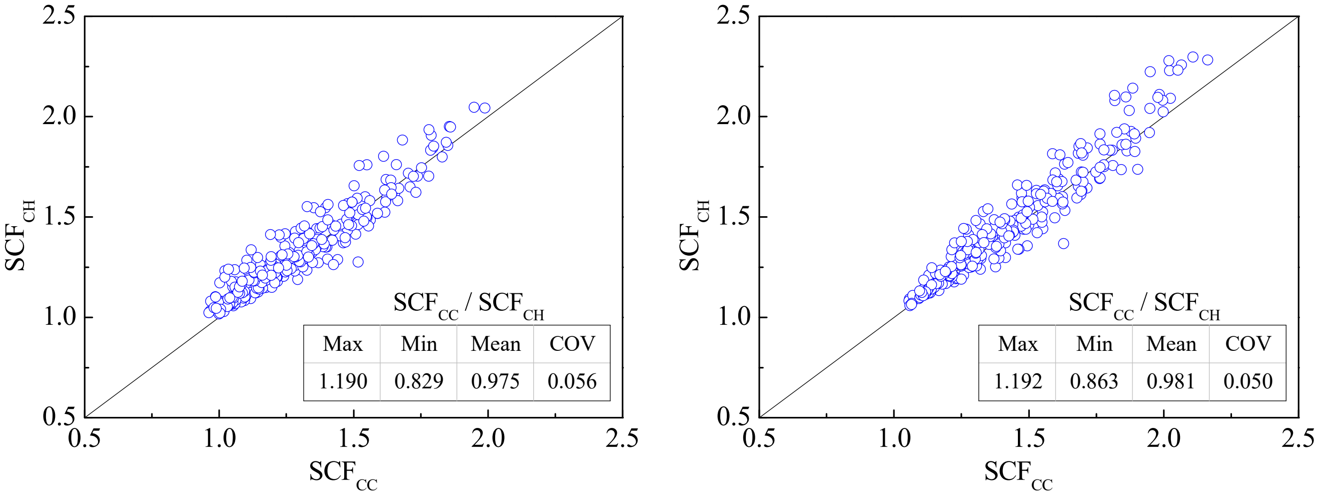

(a) Under axial compression in the chord

(b) Under in-plane bending in the chord

Fig. 11 Comparison of SCFs between locations CC and CH

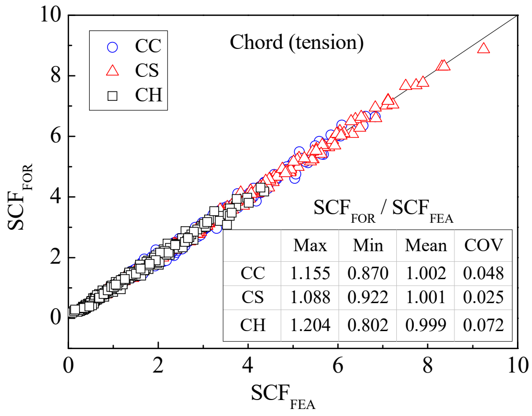

(a) Chord (tension) under basic balanced axial forces

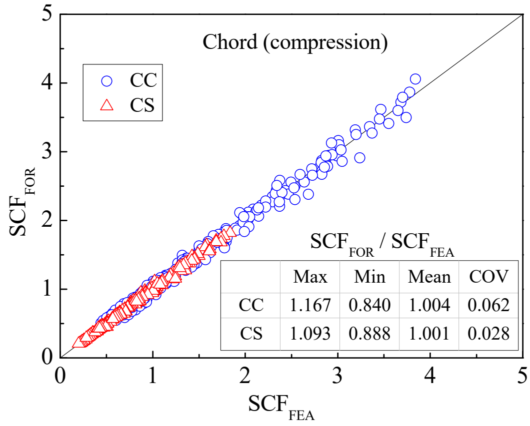

(b) Brace (tension) under basic balanced axial forces

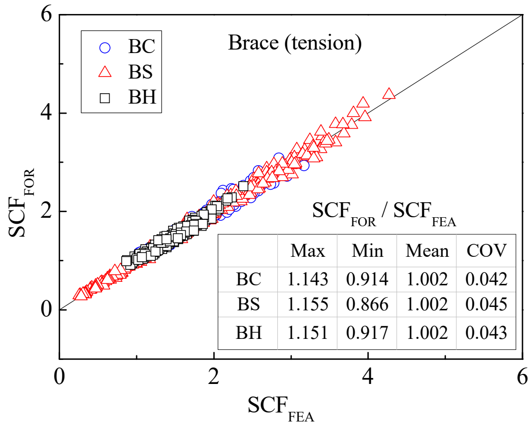

(c) Chord (compression) under basic balanced axial forces

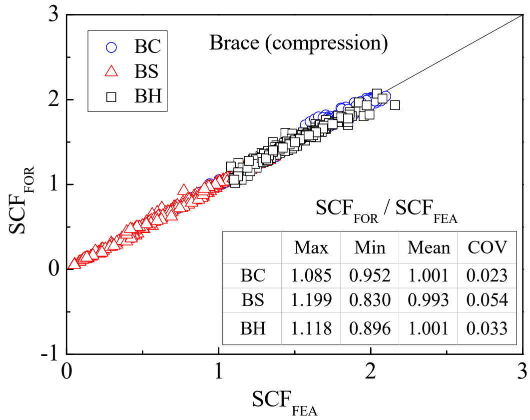

(d) Brace (compression) under basic balanced axial forces

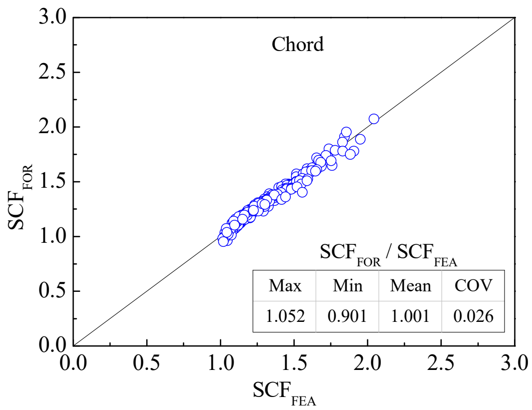

(e) Chord under axial compressive force in the chord

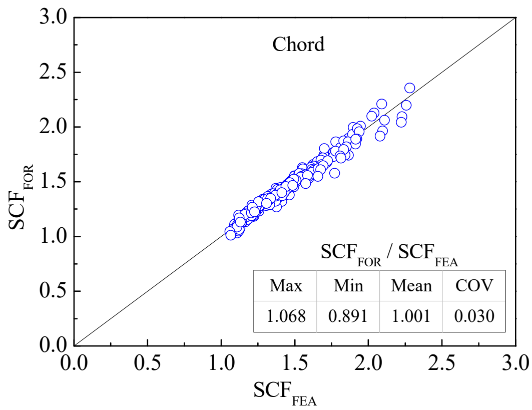

(f) Chord under in-plane bending in the chord

Fig. 12 Comparison of SCF_{FOR} with SCF_{FEA} under $\theta = 30°$, 45° and 60°

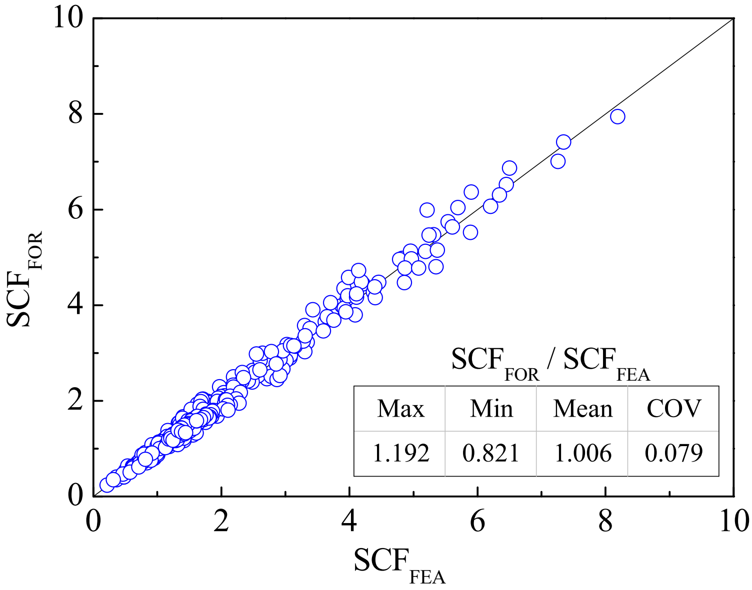

Fig. 13 Comparison of SCF_{FOR} with SCF_{FEA} under other θ-values

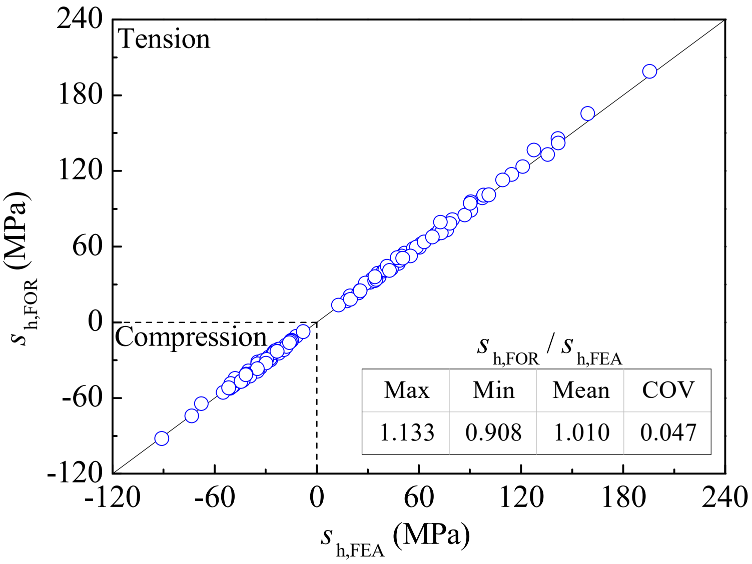

Fig. 14 Comparison of $\sigma_{h,FOR}$ with $\sigma_{h,FEA}$ under loading combination